Available online at www.sciencedirect.com
SCIENCE DIRECT®
International Journal of Heat and Mass Transfer 48 (2005) 2372–2384
International Journal of HEAT and MASS TRANSFER
www.elsevier.com/locate/ijhmt

Dendritic growth in Al–Si alloys during brazing. Part 1: Experimental evidence and kinetics

D.P. Sekulic [a,*], P.K. Galenko [b], M.D. Krivilyov [c], L. Walker [d], F. Gao [e]

[a] University of Kentucky Center for Manufacturing, College of Engineering, University of Kentucky, 521 CRMS Building, Lexington, KY 40506, USA
[b] Institute of Space Simulation, German Aerospace Center, Cologne 51170, Germany
[c] Department of Metallurgy and Materials Engineering, KU Leuven, Heverlee 3001, Belgium
[d] High Temperature Materials Laboratory, Oak Ridge National Laboratory, Oak Ridge, TN 37831, USA
[e] Collaborative Research Center for Advanced Science and Technology, Osaka University, Osaka 565-0871, Japan

Received 29 March 2004; received in revised form 25 January 2005
Available online 31 March 2005

Abstract

This work provides empirical evidence needed for an in depth phenomenological study of dendrite growth phenomena during brazing of aluminum alloys in form of composite brazing sheets. The main objective of this study was (1) a collection of experimental evidence associated with heat and mass transfer modeling of the Al + Si solid solution dendrite macro morphology evolution inherent to joint formation during brazing, and (2) the dendrite growth kinetics analysis. The isothermal dwell and the quench that follow the clad molten aluminum binary alloy surface-tension-driven flow into the joint at the peak brazing temperature upon melting lead to the solidification of the metal micro layer and joint formation. Before, during and after the isothermal dwell a significant reduction of Si content in the melt is found. So, a subsequent dissolution may affect the interface zone between the molten clad and substrate. α-phase dendrite assemblies imbedded in an irregular eutectic in the joint zone are the main morphological features of the solidification microstructures. The major characteristic of the phenomenon is a sensitivity of the dendrite pattern selection and dendrite population on brazing process parameters, in particular on the temperature during the dwell.

1. Introduction

Solidification microstructures are responsible for material's behavior in metal joining processes, such as brazing and soldering. Modification of material properties through the control of solidification microstructures is very important in a series of applications where the metal liquid—non-amorphous solid phase transition is the main feature of the process. In a variety of manufacturing processes related to netshape technologies (for example, metal joining using soldering, brazing, and/or welding) the associated quench may, in fact, be accomplished with small cooling rates. Regardless of the magnitude of the cooling rate, the dendrite solid solution crystal growth accompanied by the irregular two-phase eutectic solidification is usually present. Prediction of dendrite pattern evolution and morphological features of the solidification microstructures are the two very important issues.

* Corresponding author. Tel.: +1 859 257 2972; fax: +1 859 323 1035.
E-mail address: sekulicd@engr.uky.edu (D.P. Sekulic).

0017-9310/$ - see front matter © 2005 Elsevier Ltd. All rights reserved.
doi:10.1016/j.ijheatmasstransfer.2005.01.034

Nomenclature

C	concentration, dimensionless	T	temperature, K
m_e	liquidus slope, K/at.%	V	velocity, m/s
R	dendrite tip radius, m		

The research program summarized in these twin papers has been motivated by a need to understand the process of bond formation during metal joining associated with brazing of complex aluminum structures made of highly augmented heat transfer surfaces for, say, compact heat exchangers used in aerospace and automotive applications [1]. In Fig. 1, two characteristic joints formed between two orthogonal mating surfaces illustrate topology of the bond and indicate the two characteristic morphologies of solidification microstructures. Embedded in an irregular eutectic, the solid solution dendrite is formed during solidification executed at the end of the controlled atmosphere brazing (CAB) cycle. A dramatic difference in the population of alpha phase dendrites is the most striking feature of the two joint morphologies presented in Fig. 1. However, a less obvious seems to be a presence of fully selected dendrite patterns in cases when quench is executed from a lower temperature. Note that an imposed change of temperatures at the onset of quench for the two cases presented in Fig. 1 leads to a relatively small change in corresponding *equilibrium* liquidus Si concentration (around 1 at.%), and also a small change of the corresponding *equilibrium* alpha phase composition. However, the change of the alpha phase population reaches more than 30% when this particular small change in temperature takes place. Two issues are intertwined within this physical setting: (1) an expected change of the alpha phase presence by mass due to a change of the Si concentration in the melt leading to an increased fraction of the solid solution, *and* (2) a more subtle change in the dendrite pattern selection controlled by melt conditions at the onset of quench (or close to it). A suppressed fully developed dendrite presence in one case and an abundance of alpha phase (by mass) but not necessarily fully developed dendrite structures in another may not necessarily be attributed only to the (1) small change in the melt composition prior to solidification and/or to (2) a more pronounced solid phase fraction separation at a given temperature of the melt (as perceived by an equilibrium phase diagram). Some other mechanisms may also be responsible for this change. The key additional influence promoted by the present study is related to a major feature of this process that distinguishes it from an equilibrium solidification of a large mass of an isolated melt. In the present case, a *small* amount of Si rich melt formed from a micro layer of clad already significantly depleted in Si during the ramp-up heating of the brazing sheet, is being exposed to an isothermal dwell at the peak before the onset of quench, including a significant prolonged Si diffusion, and in some cases liquid penetration into the *massive* substrate, hence changing the state of melt. The resulting molten metal pool may become a mushy zone undercooled melt! This hypothesis will be considered in this paper. Moreover, solidification may start well before the quench.

Prediction of joint topologies in a brazing process [2,3], and associated thermal and/or mechanical integrities of the joints require a prediction of the amount of molten metal that would (1) flow into the zone of a close proximity of mating surfaces (governed by surface tension) [3], or alternately (2) the amount that will form the residue [4]. Cladding flow and joint equilibrium membrane formation precede and/or evolve concurrently before/during solidification. It is very important to notice that in the considered situation prior to solidification a significant isothermal dwell at the peak brazing temperature is usually present. This isothermal dwell could not possibly lead to the accumulation of melt in the joint zone that would attain the Si concentration established at the onset of melting (i.e., the corresponding liquidus state, as would intuitively be expected from an inspection of an equilibrium phase diagram). This is a consequence of several Si depletion mechanisms mentioned above and discussed later.

In Fig. 2, additional empirical evidence is provided to illustrate that the dominance of irregular eutectic and scarce but well developed dendrites is not a feature of a limited extent as an artifact of a particular 2D micrograph. Three successive cross-sections are shown, starting with the joint cross-section plane presented in Fig. 1(a) (the cross-section A, Fig. 2). The cross-section B was obtained by re-polishing the same sample and by shifting of the observed cross-section in the direction orthogonal to the image plane. The two successive planes are located between 38 and 89 μm (66 μm in average) apart from the plane presented in the previous cross-section, A. The third cross-section in Fig. 2, i.e. the cross-section C, is obtained after removing an additional material layer (between 120 and 170 μm, or in average about 150 μm). From Fig. 2, it is obvious that very few fully developed dendrites reside within the large volume of the joint, fully embedded in a rich eutectic, if the onset of quench is closer to the solidus of the binary alloy under investigation.

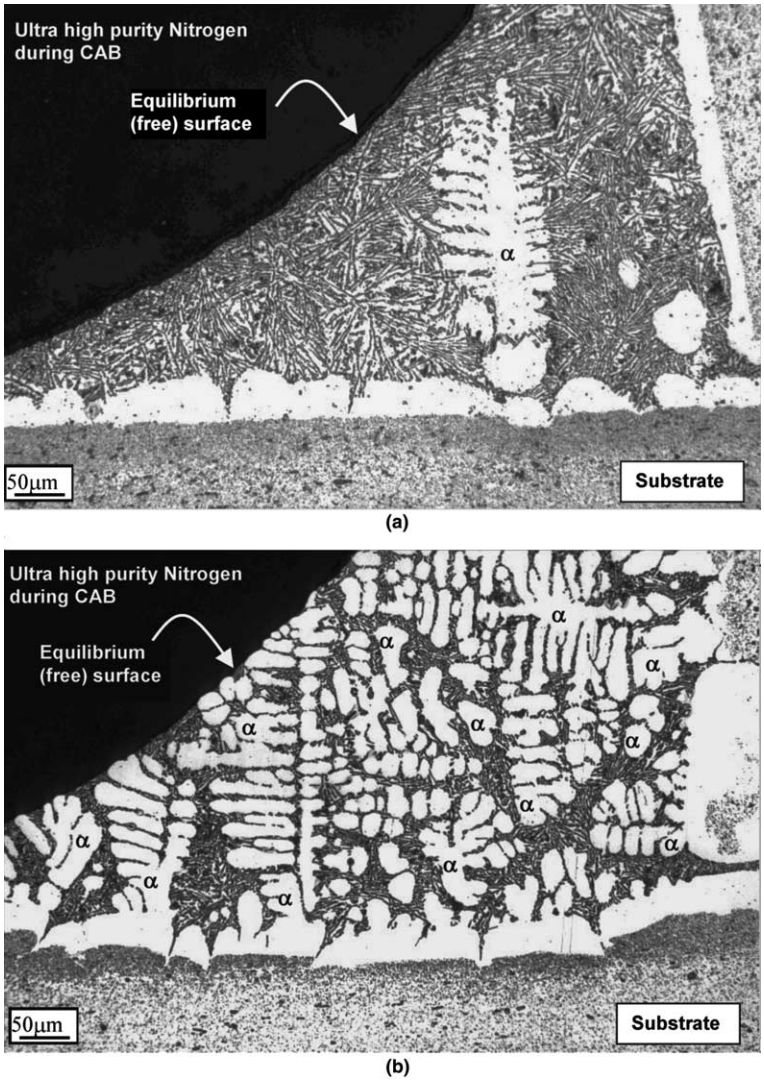

Fig. 1. Dendrite Al + Si solid solution formations imbedded in the surrounding eutectic. The samples were exposed to control atmosphere brazing (CAB): (a) dwell at 873 K, 5 min; (b) dwell at 883 K, 5 min. The brazing ramp-up, dwell, and quench temperature–time history is presented in Fig. 3.

2. Empirical evidence

2.1. Materials

Joint formation between two mating surfaces assembled in the form of inverted wedge-tee samples is created by using a brazing sheet, a composite sandwich structure consisting of a metal core and a one-sided or two-sided metal clad metallurgically attached to the core. The core and the clad of the brazing sheet considered here were made of AA3003 (lean in Si) and AA4343 (rich in Si), respectively. The brazing sheet represents the horizontal piece in a sample that has its vertical mating surface made of AA3003 (see Fig. 1). The standard composition of the core material (AA3003) and the specified chemical composition of the clad (AA4343) for two slightly different alloys are summarized in Table 1.

The brazing process consists of a sequence of three heating/cooling segments: (1) ramp up, (2) dwell and (3) quench, all in the inert nitrogen atmosphere (see also Fig. 3). Clad melts following heating during which a solid state Si diffusion across the clad–core interface starts. The melting process features non-equilibrium Si diffusion within the individual grains [5]. This is followed by a reactive flow of molten clad into joints leaving behind a residue lean in Si [4]. Finally, the liquid metal resolidifies after a dwell during which Si diffusion within the joint and into the substrate continues while

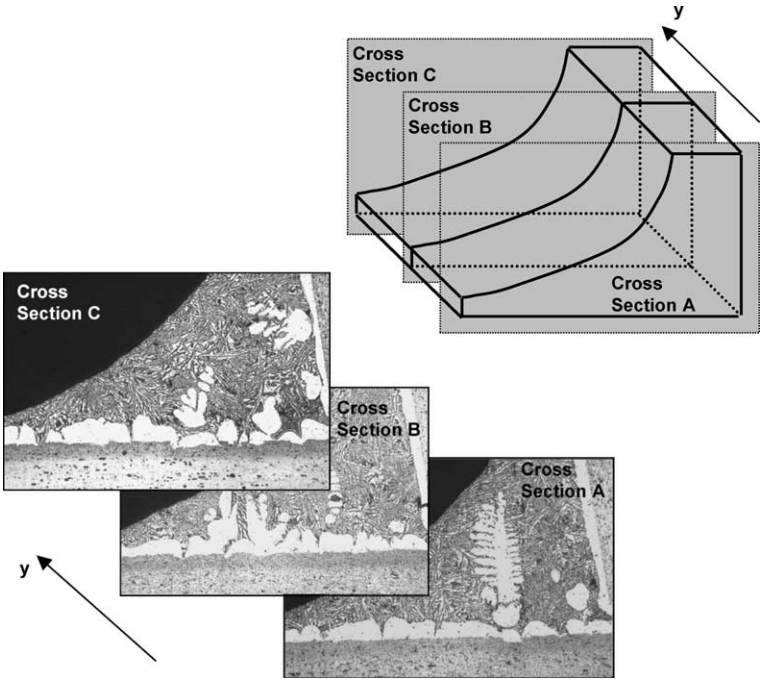

Fig. 2. Three successive cross-sections of the joint area. Cross-section A corresponds to the micrograph of the sample presented in Fig. 1(a). Cross-sections A and B are in average 66 μm apart. The cross-section C is in average 150 μm apart B.

Table 1
Cladding (AA4343) average compositions (measured) and core (AA3003) standard composition, wt%

Material[a]	Si	Fe	Cu	Mn	Mg	Cr
AA4343c	6.523	0.133	0.003	0.002	0.005	0.001
AA4343d	7.192	0.160	0.027	0.015	0.004	0.001
AA3003	<0.6	<0.7	0.05–0.2	1.0–1.5	–	–

[a] Designators "c" and "d" indicate not only the difference in composition, but also that different casting methods were used in manufacturing these two materials.

sometimes associated with base metal dissolution, liquid penetration, and ultimately with substrate erosion (Fig. 4). In the molten phase, the melt is, indeed, not of the same composition as the solid clad before melting due to the addition of flux (potassium fluoroaluminate, less than 10 g/m^2) and, more importantly, due to various competing diffusion and reaction processes present during the brazing process. Our approach to modeling of the melt solidification will be conducted for various effective compositions of the molten clad, spanning from a nominal value close or equal to initial concentration, to the corresponding liquidus value of Si enriched melt collected in the joint. The issue of the melt composition at the onset of solidification will be discussed later. Regardless of the composition, it should be mentioned that the molten metal properties at the onset of solidification may be assumed to be uniform within physically limited-size (sufficiently small) region of interest, in accord with effective molten aluminum alloy properties at the end of dwell at the peak brazing temperature. The experiment demonstrated unequivocally that the Si depletion may be so intense that at the later stages of an isothermal dwell the Si diffusion controlled solidification may start well before the onset of quench, leading to a presence of a mushy phase within the joint area that may even become undercooled.

In Fig. 4 the sequence of micrographs and the Electron Probe Micro Analyzer (EPMA) maps of the interface between the clad and core both far from the joint and in the joint zone are presented. It is important to notice (see Fig. 4(a)), that silicon initially present in the clad alloy primarily in a form of distinct particles diffuses within the clad and subsequently into the core at elevated temperatures (i.e., a solid state diffusion takes place, see Fig. 4(b)). The migration of Si causes its redistribution in the clad and core—the clad becomes leaner and the substrate richer when compared to the initial clad composition. Note a significant Si penetration of the order of magnitude of 10^2 μm into the substrate, see Fig. 5(a) and (b). Even more importantly, during the dwell at the peak brazing temperature, Si diffusion continues, and substrate dissolution and related core metal erosion dilute the Si rich melt prior to quench, forcing it to lose Si at the given constant temperature

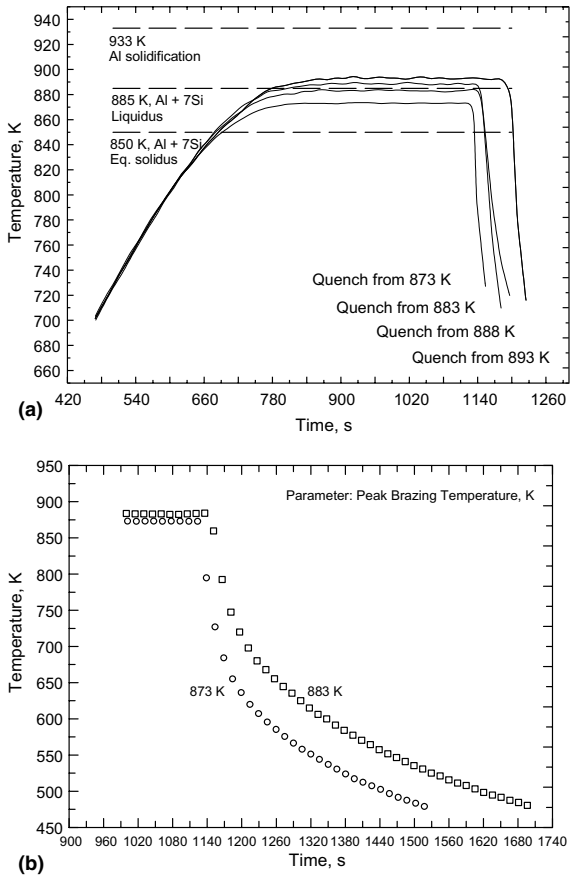

Fig. 3. (a) Temperature–time history for several ramp-up/dwell heating-melting segments and subsequent quench. The equilibrium temperatures for liquidus and solidus are indicated. Cladding sheet surface temperature in the vicinity of the joint is in the range of 873 and 893 K with 5 K increments; (b) Quench from the peak brazing temperature. Dwell at peak brazing temperatures (873 and 883 K) was in both cases 5 min. Quench conducted by convective flow of nitrogen. Peak brazing temperature maintained by radiation heating.

imposed by tightly controlled experimental conditions. So, a series of complex transient phenomena, in particular diffusion processes, sets the stage for the formation of microstructures during re-solidification. In the adjacent substrate near the clad–core interface, Si concentration increases and that increased silicon content reduces the liquidus temperature locally, thus opening the way for liquid penetration/erosion when the sample dwells at the peak brazing temperature (see Fig. 4(c), and in particular the joint zone in Fig. 4(d)). Molten clad solidification far from the joint (Fig. 4(c)) and in the joint zone (Fig. 4(d)) leads to characteristic solid solution (alpha phase) formations, and solid solution plus eutectic microstructure formations, respectively. As can be seen from the EPMA maps, Si-rich liquid penetrates along the larger solid solution grains, and/or already more or less formed α-phase dendrites. It is important to notice that a typical dendritic structure (see also Fig. 1) forms exclusively within the joint zone. As seen from Fig. 1(a), the dendrite starts forming and evolves within the zone adjacent to the substrate where the Si diffusion and dissolution are the more pronounced and the effective melt undercoolings most probably the most prominent. The residue formation far from the joint features a very little eutectic (if the solidification is preceded by the surface-tension-driven molten cladding flow (as is the case in Fig. 4(c))), and the plate-like structures of α-phase, occasionally interrupted by penetrated liquid metal that could not be dragged into the joint by surface tension [4].

Our interest in this study was directed primarily to the solid solution formation in the joint area where the melt is in abundance. In Fig. 5, a clear proof of Si concentration reduction in the melt prior to solidification can easily be devised from Si concentration profiles at the interface between subsequently formed solid state and the substrate. One can find more details about the related diffusion processes involving the experimental conditions identical to the ones used in this study in [6].

2.2. Experimental procedure

Each sample was exposed to a brazing sequence in a laboratory furnace with a transparent computer controlled hot zone. The schematic of the hot zone configuration is presented in Fig. 6. Heating was in all cases conducted by radiation (symbolized in Fig. 6 by the electric heater ring around the hot zone), and in the presence of a constant mass flow rate $(3–4)\times 10^{-3}$ kg/s of nitrogen with ultra-high purity of 99.999%. Cooling during the quench was performed by nitrogen forced convection and radiation heating turned off. Solidification is a consequence of (primarily) conduction of heat away from the joint zone through mating surfaces, acting as very efficient thermal energy dissipating devices at an onset of rapid flow of an additional nitrogen stream at the start of quench. The dwell temperature, as well as the quench conditions, may differ from test to test but were pre-determined and fixed during each experiment. In all tests, the dwell time was kept constant (5 min), (Fig. 3). The range of sample temperatures at peak brazing temperature levels was kept between 873 and 893 K. Temperatures were measured at the AA3003 sheet surface by using a pair of thermocouples (the uncertainty in temperature measurements was less than ±0.5 K). A computer, using feedback provided by one of the two surface-attached thermocouples, guided the sample temperature profile. The ramp-rate was kept in the range of up to 40–50 K/min. The quench was initiated at the expiration of the pre-determined dwell time. The onset of the additional nitrogen stream flow at the beginning of quench (99.9 nitrogen at room temperature) was

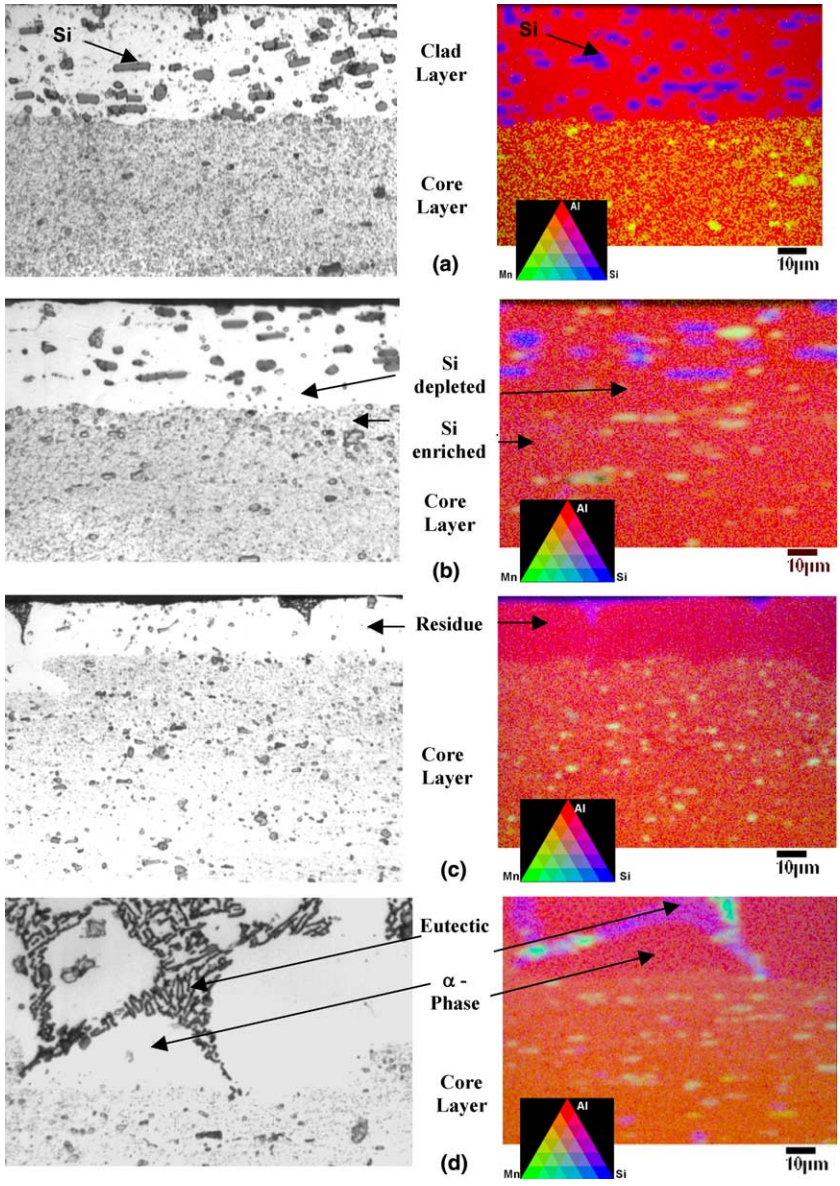

Fig. 4. Micro layer of cladding: (a) at room temperature (300 K); (b) before the onset of melting at the elevated temperature (843 K); (c) after re-solidification far from the joint (quench from 878 K after a 5 min dwell); (d) after re-solidification in the joint zone (quench from 878 K after a 5 min dwell). Magnification at the micrographs approximately the same as in the EPMA maps.

triggered upon completion of the dwell time. The nitrogen stream jet was directed toward the sample and maintained at a constant mass flow rate until the temperature of the sample reached around 600 K. Subsequently, the cooling was conducted by free convection, first in nitrogen and then in air, until the test coupon reached the room temperature.

The specimens to be analyzed were formed by cutting equally sized segments out of the brazed wedge-tee samples, and subsequently by embedding the machined segments in resin, thus forming metallographic samples. This is accomplished by using the cold mounting EPOVACK® vacuum impregnation procedure that allows for a negligible change of the joint zone topology. Each sample is cleaned in an ultrasonic cleaner and rinsed with ethanol. The hardening is conducted at room temperature to prevent any shrinkage. The sequence of grits used for polishing was 320, 500, 1200, and 4000 followed by a 3 μm diamond suspension and a 0.04 μm silicon suspension. Polishing was accomplished using a smart

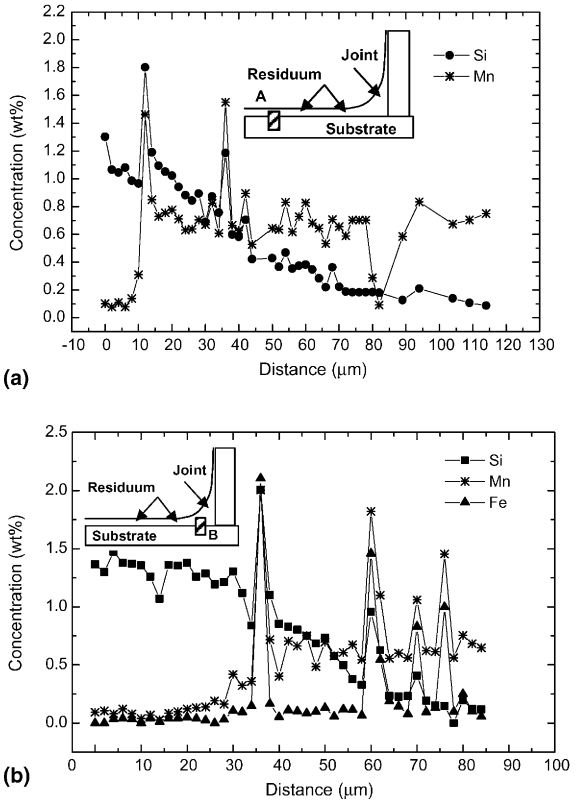

Fig. 5. Diffusion of Si at the interface; (a) Sample T21, quench from 878 K, dwell time at 878 K is 5 min; (b) Sample T11, quench from 878 K, dwell time at 878 K is 5 min.

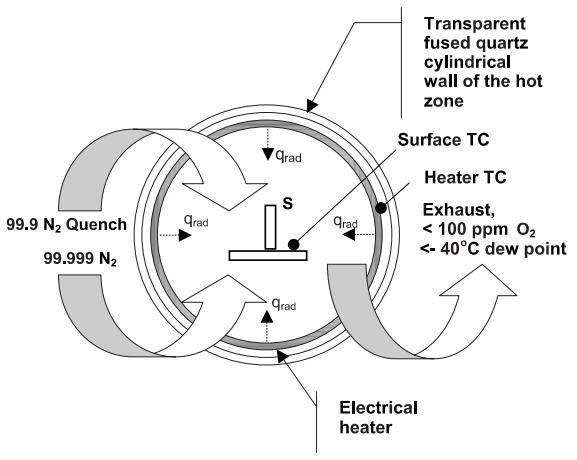

Fig. 6. Schematic of the experimental set-up configuration. A sample located in the transparent hot zone is heated by an electrical heater and exposed to a steady flow of ultra-high purity nitrogen. During quench, a nitrogen jet cools the sample by forced convection. Here, TC—thermocouple positions; S—sample; q_{rad}—the heat flux due to radiation.

grinder/polisher and specimen mover. Before each set of light microscopy measurements, the samples were etched using Keller's reagent (2 ml HF + 3 ml HCl + 5 ml HNO_3 + 190 ml H_2O). Subsequently, the joint zone with solidification structures was analyzed using (i) an optical inverted metallurgical microscope (equipped with a digital image retrieval and processing software, Image Pro Plus® V4.1), (ii) the scanning electron microscopy and EDX (with and without etching), and (iii) the electron microprobe analysis, i.e., EPMA (etching removed to eliminate contamination).

2.3. Solidification microstructures

In Fig. 7, a series of micrographs illustrates the macro morphology of solidification microstructures formed during CAB joint formation. Each micrograph is identified with the value of the peak brazing temperature—also a starting point for the quench. When sequenced in descending order of the peak brazing temperature, the resulting solidification microstructure morphology shows a change: starting with 893 K, the joint zone is characterized with a very rich population of dendrite structures of the alpha phase with very little irregular eutectic surrounding the dendrites.

Morphological features of the alpha phase/eutectic microstructures, starting with a high temperature of melt in the liquid range, do not change significantly with the decrease of the peak brazing temperature until the dwell temperature reaches a level below the corresponding equilibrium liquidus temperature (which is 885 K for the initial concentration of the given Al + Si alloy). Pattern selection of the dendrites is not necessarily clearly manifested within the whole joint area, in particular far from the interfaces. However, further decrease of temperature at the onset of quench up to the 873 K level leads to a steady decrease in dendrite structure density population and an increase in the volume of eutectic, but the pattern selection of individual dendrite structures appears to be more obvious. At 873 K dendrites are scarce but fully developed (see Fig. 1(a)) or alternately even non-existent in a given cross-section (see Fig. 7).

One may be tempted to provide a straightforward and simple answer for such a morphology evolution. Namely, melt at a given temperature, if the conditions associated with the construction of a corresponding equilibrium phase diagram for Al–Si system are assumed as valid, should correspond to the alloy equilibrium state at the related liquidus line. An increase in temperature prior to quench would lead to an increase in Al content thus leading to more populated alpha phase dendrite structures.

This intuitive (and plausible) explanation does not take into account that the melt, when produced, cannot be at its equilibrium liquidus concentration at the given

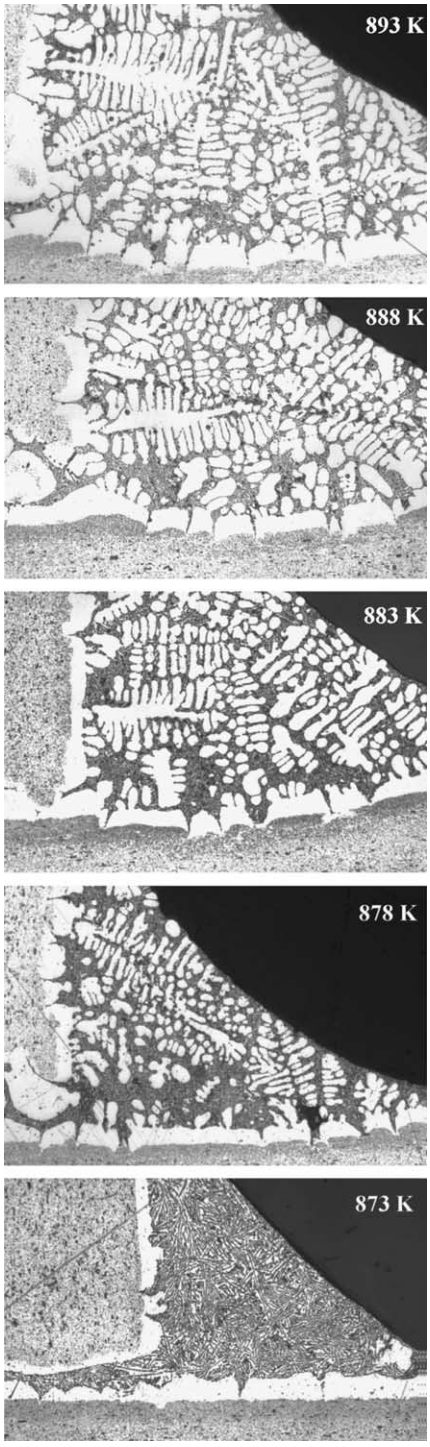

Fig. 7. A series of micrographs of the joint zone featuring solidification microstructures formed at different peak brazing temperatures. An increase in peak brazing temperature leads to the more pronounced dendritic alpha phase formations and less of the surrounding irregular two phase eutectic. Magnification 200× (reduced in print).

temperature due to two reasons: (1) melting of Al grains is diffusion controlled and the produced melt Si concentration decreases with the increase of temperature but being steadily even higher than the corresponding liquidus temperature, (2) the presence of Si diffusion, and the other Si loss mechanisms discussed above like core dissolution, provide conditions for a mushy melt. An exact melt concentration at the onset of solidification in the clad close to interface cannot be measured in situ at the present level of sophistication of experimental procedures. The a posteriori measurements indicate that the resulting heterogeneous structure concentration has a trend of Si decrease with the increase of peak temperature (as expected), but, the Si concentration is even larger than the liquidus value for the corresponding onset of quench temperature due to a very high Si concentration within the needle like crystals formed from a close to eutectic melt, but far from the clad core interface (i.e., at the levels of 17, 13, 12 and 10 wt% for 873, 878, 883 and 888 K, the other conditions as elaborated in Section 2.2). The measurements of bulk concentrations were conducted using the electron dispersive X-ray analysis for mapping of the central portions of the joints. However, the measurements of various elements distributions *in the interface zones* (conducted by electron microprobe scans and maps, see Figs. 4 and 5) indicate dramatically lower Si concentrations.

Hence, it is plausible to assume that actual Si concentrations at the onset of solidification are spatially dependent, i.e., distinct on the macro scale but more-or-less locally homogeneous within different joint zone areas. In our study, a hypothesis will be formulated that the Si diffusion and dissolution mechanisms, well documented and thoroughly studied here and elsewhere, may lead to a smaller or larger undercoolings in physical domains comparable to the scales of initial dendrite formations (close to the interface region in particular). The nominal values of Si concentration will be in a range between 6.93 at% (initial concentration limit) and 8.5 at% (a close to liquidus limit) at 873 K, and 5.5 and 6.9 at% at 883 K. These ranges produce undercooling levels between 4 K (low) and 14 K (high). As will be demonstrated through numerical modeling later [19], different undercoolings, to which the samples with peak brazing temperatures in descending order are *assumed* to be exposed, play a role in forming the familiar dendrite pattern.

3. Problem statement

Liquid or semi-liquid melt is exposed to a quench following a pre-defined temperature–time history, Fig. 3. An isothermal dwell at the peak temperature, with a simultaneous Si removal from the melt due to Si diffusion and

substrate dissolution, may cause undercooling (various degrees to be considered) of the melt at the melt–substrate interface, hence may lead to a shift away from both the corresponding equilibrium liquidus concentration and a nominal concentration prior to quench. The additional goal of modeling would be to mimic the dendrite microstructure transient formation and to predict the main features of dendrite growth kinetics. Whether the modeling approach is sensitive enough to mimic the difference in the pattern formation during solidification at different cooling rates and quench temperatures as presented in Fig. 7 will be analyzed subsequently (see Part 2, [19]).

For detailed modeling of dendritic structure we shall develop a model of the two-phase mushy zone which will provide the non-isothermal extension of the recently suggested model for isothermal crystal growth [7,8]. This problem is the subject of Part 2 of this paper [19]. For evaluation of the kinetics of dendritic growth we shall use the model of rapid dendritic growth based on the local non-equilibrium approach [9,10].

4. Kinetics of the dendrite growth

The model of a free-dendrite growth can be utilized to describe growth of a single dendrite, as disclosed here by the experimental evidence in Fig. 1(a). It is expected that this model will provide adequate prediction of the main characteristics of the dendrite structure. Regarding the growth of an ensemble of the dendrite pattern (as shown in Fig. 7), an additional assumption is required. Namely, one shall assume that temperature and concentration fields of dendrites do not overlap, at least during the stage of the steady-state growth of an initially precipitated alpha phase. Further, it should be mentioned that the model used describes both rapid and slow solidification as it might be considered for the limiting cases of a large and a small undercoolings, respectively. Therefore, one can apply this model to a whole range of undercoolings and crystal growth velocities relevant for the aluminum alloy brazing "rapid quench" considered in this study (the word "rapid" in this statement does not necessarily refer to a "rapid solidification" but rather to a sluggish phase change).

4.1. Kinetics of 2D dendrite growth

In order to establish the kinetics of the related dendrite solidification in the Al–Si system under consideration, a model for dendrite growth from undercooled binary alloy is developed. This model will be applied to a 2D steady-state dendrite growth. In a 2D steady-state dendrite growth, the dendrite moves into an undercooled molten alloy with a constant velocity V in the selected direction and has a steady-state tip radius R. The 2D crystal growth shape formulation and solution for concentrational distribution are derived in [11].

The basic equations of the 2D dendrite growth model are established as follows. The total undercooling ΔT in the liquid ahead of the advanced dendrite interface is described by

$$\Delta T = T_A + m_e C_0 - T_0 = \begin{cases} \Delta T_T + \Delta T_R + \Delta T_C + \Delta T_N + \Delta T_K, & V < V_D, \\ \Delta T_T + \Delta T_R + \Delta T_N + \Delta T_K, & V \geqslant V_D. \end{cases} \tag{4.1}$$

In the definition of the total undercooling, T_A and T_0 represent equilibrium solidification temperature of the main component of the alloy (aluminum) and the temperature far from the solid–liquid interface, respectively. The undercooling contributions included in Eq. (4.1) and Fig. 8 are listed in Table 2.

One of the distinguished features of the system of equations defining the undercoolings (see Table 2) is the absence of the constitutional undercooling ahead of the dendrite tip at finite velocities $V \geqslant V_D$. The consequence is that $\Delta T_C = 0$ at $V \geqslant V_D$, due to the equality, $C_I = C_0$, which follows directly from the two-dimensional solution for the solute distribution [11]. In Table 3, the solute distribution, the interface concentration, the related solute partitioning coefficient [12], and the slope of the non-equilibrium liquidus line as a function of non-equilibrium partitioning k and crystal growth velocity V [13] are compiled. The slope m of the kinetic liquidus (Table 3) has been obtained [13] by using a formalism of extended irreversible thermodynamics [14].

The set of undercooling equations given in Table 2 secures a correlation between the undercooling ΔT and the product of VR. A unique determination of V as a function of ΔT can be obtained from the linear stability analysis for the planar solid–liquid interface in the case of local non-equilibrium mass transfer [9] (see Table 3). Note that the function ξ_C of the concentrational stability differs significantly from the function found by means of the local equilibrium approach used for modeling of the mass transfer in rapid solidification [15]. When $V \ll V_D$, the expression for R coincides with those obtained by using the local equilibrium approach to solute diffusion [15]. When the velocity V is of the order of the diffusion speed V_D, the function ξ_C includes the diffusion speed. When $V \geqslant V_D$, ξ_C is zero exactly. Thus, expression for R predicts the complete transition to thermally controlled radius of the dendrite tip with the finite velocity which is equal to or higher than the diffusive speed in the bulk liquid, $V \geqslant V_D$.

4.2. Predictions of the model of dendrite growth kinetics

In general, the model presented in Section 4.1 reduces to the existing theories for $V_D \to \infty$ (i.e. for the case of

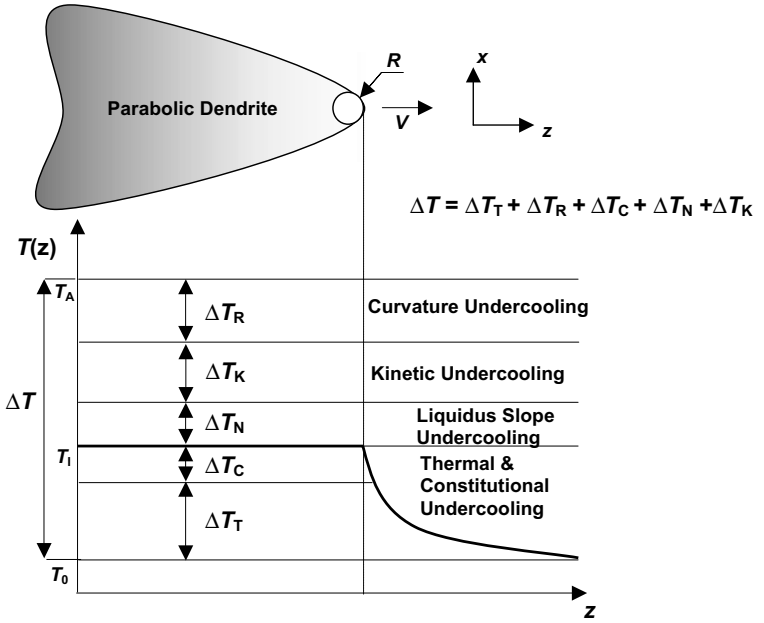

Fig. 8. Schematic presentation of the 2D parabolic thermal and solutal dendrite growing into an undercooled melt. A thermally controlled growth is possible for an alloy solidification characterized with $V \geqslant V_{\mathrm{D}}$, the undercooling due to the change of the slope of liquidus $\Delta T_N = \text{const.}$, and the constitutional undercooling $\Delta T_{\mathrm{C}} = 0$.

Table 2
The undercooling components

Undercooling	Relationship[a]	Meaning and comments
ΔT_T	$\Delta T_T = T_I - T_0 = \frac{Q}{\kappa}\mathrm{Iv}(P_T)$	Thermal undercooling at the tip of dendrite
ΔT_R	$\Delta T_R = \frac{\Gamma_0(1-15\varepsilon_\Gamma\cos 4\theta)}{R}$	Curvature undercooling caused by Gibbs–Thomson effect at the tip of dendrite
ΔT_{C}	$\Delta T_C = \begin{cases} m[C_0 - C_I] = -mC_0\dfrac{(1-k)\mathrm{Iv}(P_C)}{1-(1-k)\mathrm{Iv}(P_C)}, & V < V_D, \\ 0, & V \geqslant V_D \end{cases}$	Constitutional undercooling at the tip due to solute presence
ΔT_N	$\Delta T_N = (m_e - m)C_0$	$\Delta T_N = T_E - T_N = (T_{\mathrm{A}} + m_e C_0) - (T_{\mathrm{A}} + mC_0)$ Undercooling due to a shift from equilibrium liquidus
ΔT_K	$\Delta T_K = V/\mu_0$	Kinetic undercooling

[a] The following additional symbolism is adopted: V and R are the dendrite tip velocity and radius, respectively, T_I and C_I are the temperature and the liquid concentration at the dendrite tip, respectively, $P_T = VR/2a$ is the thermal Peclet number, $P_{\mathrm{C}} = VR/2D$ is the solutal Peclet number, $\mathrm{Iv}(P_i) = (\pi P_i)^{1/2}\exp(P_i)\mathrm{erfc}(P_i^{1/2})$ is the Ivantsov-function for the 2D dendritic growth ($i = T$ or C), m is the slope of the non-equilibrium liquidus line, and k is the partition coefficient dependent on V. All other parameters and constants are specified in Table 1 of [19].

local equilibrium solute diffusion, i.e., the classic Fick's approximation) and gives new qualitative and quantitative predictions if V_{D} is finite. First, if $\mathrm{Iv}(P_T) = 1$, $\mathrm{Iv}(P_C) = 1$, and $R \to \infty$, this model describes rapid solidification with planar interface motion [16]. Second, as soon as $V \ll V_{\mathrm{D}}$, the set of equations of the model (Tables 2 and 3) can be reduced to the LKT/BCT model for calculation of the dendrite tip velocity and radius under local equilibrium solute diffusion [17,18].

As particular cases of the present 2D model one may distinguish three regimes of the dendritic growth:

(i) diffusion-limited growth (solutal dendrite);
(ii) diffusion-limited and thermally controlled growth (solutal and thermal dendrite);
(iii) purely thermally controlled regime (thermal dendrite).

For instance, case (ii) is presented schematically in Fig. 9 where the solutal and thermal dendritic platelet is growing into the undercooled melt. Note that with the finite growth velocity $V = V_{\mathrm{D}}$ and with the absence of the constitutional undercooling, a sharp transition

Table 3
Solute distribution and auxiliary parameters

Entity	Relationship		Comments[a]
	$V < V_{\mathrm{D}}$	$V \geqslant V_{\mathrm{D}}$	
C	$C_0 + (C_I - C_0)\dfrac{\operatorname{erfc}[(P_{\mathrm{C}}u)^{1/2}]}{\operatorname{erfc}[(P_{\mathrm{C}})^{1/2}]}$	C_0	$u = \dfrac{z - Vt + [(z-Vt)^2 + (1 - V^2/V_{\mathrm{D}}^2)x^2]^{1/2}}{R(1 - V^2/V_{\mathrm{D}}^2)}$
C_I	$\dfrac{C_0}{1 - (1-k)(\pi P_{\mathrm{C}})^{1/2}\exp(P_{\mathrm{C}})\operatorname{erfc}[(P_{\mathrm{C}})^{1/2}]}$	C_0	$z - Vt = \dfrac{R(1 - V^2/V_{\mathrm{D}}^2)}{2}\left(1 - \dfrac{x^2}{R^2(1 - V^2/V_{\mathrm{D}}^2)}\right)$
k	$\dfrac{k_e(1 - V^2/V_{\mathrm{D}}^2) + V/V_{DI}}{1 - V^2/V_{\mathrm{D}}^2 + V/V_{DI}}$	1	A generalization of the continuous growth model (see [21]) for the case of local nonequilibrium solute diffusion
m	$\dfrac{m_e}{1 - m_e}\left[1 - k + \ln(k/k_e) + (1-k)^2(V/V_D)\right]$	$\dfrac{m_e \ln(1/k_e)}{1 - k_e}$	Note that for $V_{\mathrm{D}} \to \infty$ (a limit of the local equilibrium of solute diffusion) m transforms in an expression in which the solute-drag effect in rapid interface motion has been taken into account [21]
R	$\dfrac{\Gamma_0(1 - 15\varepsilon_\Gamma\cos 4\theta)}{\sigma^*}\left[T_Q P_T \xi_T - \dfrac{2m(1-k)C_0 P_{\mathrm{C}}\xi_{\mathrm{C}}}{(1 - V^2/V^2 D)[1 - (1-k)\mathrm{Iv}(P_{\mathrm{C}})]}\right]^{-1}$	$\dfrac{\Gamma_0(1 - 15\varepsilon_\Gamma\cos 4\theta)}{\sigma^* T_Q P_T \xi_T}$	$\xi_T = 1 - [1 + 1/(\sigma^* P_T^2)]^{-1/2}$
			$\xi_{\mathrm{C}} = \begin{cases} 1 + \dfrac{2k}{1 - 2k - [1 + (1 - V^2/V_{\mathrm{D}}^2)/(\sigma^* P_C^2)]^{1/2}}, & V < V_{\mathrm{D}}, \\ 0, & V \geqslant V_{\mathrm{D}} \end{cases}$

[a] The entity σ^* is defined as $\sigma^* = \sigma_0 \epsilon_I^{7/4}$, and represents the parameter of stability defined by the solvability condition for the relatively sluggish growth kinetics Refs. 19 and 21 in [19]. ξ_{i} are the stability functions ($i = T$ or C). The other entities and the corresponding symbols are provided in Table 2 and Table 1 of [19].

from solutal and thermal dendrite to the thermal dendrite exists, i.e. only the purely thermally controlled solidification occurs with $V \geqslant V_D$. Such thermal growth is governed by the heat removal out from the dendritic interface with the increasing influence of the kinetic undercooling and at the constant value of liquidus slope undercooling.

In order to predict the steady-state dendrite growth, the following two analyses were performed: (1) the "velocity vs. undercooling relationship" calculation, and (2) the "dendrite tip radius vs. undercooling" calculation. The calculations were performed using the system of equations given in Tables 2 and 3. This system features two nonlinear algebraic equations, one for undercooling and the other for the tip radius, which provide the expressions for the required calculation of the dendrite tip radius R and dendrite tip velocity V as the main characteristics of the primary dendritic structure. With an increase of the initial undercooling ΔT, the dendrite tip radius R decreases monotonically within the range (i) of the diffusion-limited growth; then it sharply increases, reaching its maximum value within the range (ii) of the diffusion-limited and thermally controlled growth, and finally it decreases monotonically with a break at the point $\Delta T(V_D)$ within the range (iii) of the purely thermally controlled growth. The calculated kinetic "velocity vs. undercooling" curve for the dendrite solidification in a Al–Si alloy is shown in Fig. 9 (additional data required for this calculation are provided in Part 2, [19], Table 1).

As it can be seen from Fig. 9, the velocity vs. undercooling relationship exhibits a single-valued curve, i.e.

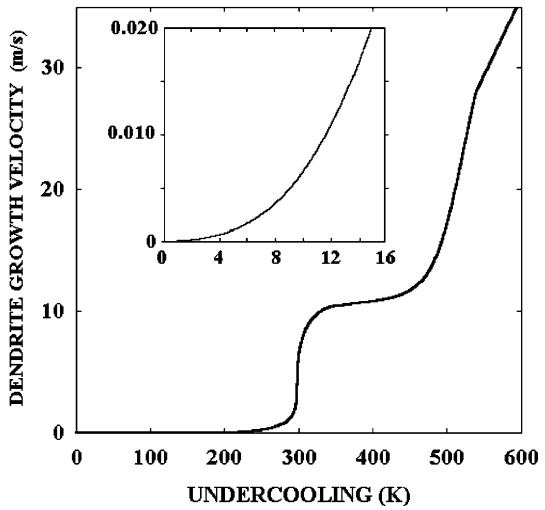

Fig. 9. The kinetic curve featuring the dendrite tip growth velocity V vs. undercooling ΔT. The inset shows the same relationship in the region of the undercooling investigated in this paper. Note that the abscissa in inset shows the velocity in mm/s.

for any value of the undercooling, there is only one value of the dendrite growth velocity. According to the methodology presented in [20], such a single-valued curve gives a dynamically stable regime of crystal growth around any point of the steady-state relationship. One would expect that in the modeling of the microstructure formation, after the stage of the transient non-steady solidification, the steady-state regime would proceed in the alloy and it could be described by the steady kinetic curve showed in Fig. 9.

From Fig. 7 one can learn that the peak brazing temperature from which solidification may start is in the range 873–893 K. Comparing these temperatures with the appropriate liquidus temperature for the Al–Si alloy, one would predict that the maximum undercooling for the present brazing "rapid quench" may (theoretically) reach values definitely not higher than $\Delta T \approx 20$ K. Following the kinetic curve indicated in Fig. 9, such the undercooling provides a steady-state velocity lower than or around 0.02 mm/s. Therefore, one can conclude that the quenching accomplished within the present experimental conditions may provide a sluggish solidification kinetics.

5. Conclusions

Solidification of molten Al + Si cladding within a CAB brazing cycle may lead to a scarce population of α-phase solid solution dendrites within the rich irregular eutectic (melt exposed to relatively low temperature at the onset of quench and in the presence of Si depletion at the constant temperature dwell before the quench). However, a fully selected dendrite pattern is often present, developing from the interface zone. In contrast, if the initial temperature is relatively high in the mushy zone, or if the quench starts from the melt above the liquidus, the population of dendrites is large and no clearly defined dendrite patterns within the bulk phase were noticed (as opposed to the close to interface zones). The dendrites grow from the interface zones exposed to Si diffusion and core dissolution before the quench.

Velocity-undercooling relationship exhibits a one-to-one correspondence between the undercooling level and the dendrite growth velocity, leading to a stable regime of a dendrite growth. The undercooling level reached in the present brazing of Al–Si alloy has lead to the conclusion that the crystal growth in the region of investigated peak brazing temperatures provides relatively sluggish kinetics of solidification under the diffusion-limited stage of crystal growth.

Acknowledgements

The National Science Foundation has provided support through the NSF Grant DMI-9908319, monitored

by Dr. Delcie Durham and Dr. Julie Chen. P.K. Galenko acknowledges support from the Alexander von Humboldt Foundation through the research program no. IV RUS 1068584. A portion of this work was supported by Assistant Secretary for Energy, Office of Transportation Technologies, as part of the High Temperature Materials Laboratory user program at ORNL, managed by UT—Battelle, LLC, for the US DOE under contract # DE-AC05-00OR22725 through the project #UA-90-015. One of the co-authors (GF) would like to express his appreciation for the support provided by CRMS, College of Engineering at the UK through a research assistantship. Numerical calculations were performed in part thanks to support from the University of Kentucky Computing Center and the University of Kentucky Center for Computational Sciences (CCS) that operates within the framework of the National Center for Supercomputing Applications (NCSA).

References

[1] R.K. Shah, D.P. Sekulic, Fundamentals of Heat Exchanger Design, Wiley, New York, 2003.

[2] B.P. Zellmer, N. Nigro, D.P. Sekulic, Numerical modeling and experimental verification of the formations of 2D and 3D brazed joints, Modell. Simul. Mater. Sci. Eng. 9 (2001) 339.

[3] D.P. Sekulic, F. Gao, H. Zhao, B. Zellmer, Y.Y. Qian, Prediction of the fillet mass and topology of aluminum brazed joints, Welding J. 83 (3) (2004) 102–110.

[4] F. Gao, D.P. Sekulic, Y.Y. Qian, J.G. Morris, Formation of microlayers of clad residue on aluminum brazing sheet during melting and resolidification in brazing process, Mater. Sci. Technol. 20 (4) (2004) 1–8.

[5] H. Zhao, D.P. Sekulic, Modeling of the influence of a microstructure scale on the re-solidification of micro-layers of a molten aluminum alloy. in: Proc. of the Fourth Int. Symp. on Scale Modeling ISSM-IV, Cleveland, Ohio, 2003, NCRM-NASA Glen Research Center, pp. 291–301.

[6] F. Gao, Z. Hui, D.P. Sekulic, Y. Qian, L. Walker, Solid state Si diffusion and joint formation involving aluminum brazing sheet, Mater. Sci. Eng. A 337 (2002) 228–235.

[7] P.K. Galenko, M.D. Krivilyov, Model for isothermal pattern formation of growing crystals in undercooled binary alloys, Modell. Simul. Mater. Sci. Eng. 8 (2000) 67–79.

[8] P.K. Galenko, M.D. Krivilyov, Modelling of crystal pattern formation in isothermal undercooled alloys, Modell. Simul. Mater. Sci. Eng. 8 (2000) 81–94.

[9] P.K. Galenko, D.A. Danilov, Local nonequilibrium effect on rapid dendritic growth in a binary alloy melt, Phys. Lett. A 235 (1997) 271–280.

[10] P.K. Galenko, D.A. Danilov, Model for free dendritic alloy growth under interfacial and bulk phase nonequilibrium condition, J. Cryst. Growth 197 (1999) 992–1002.

[11] P.K. Galenko, D.A. Danilov, Steady-state shapes of growing crystals in the field of local nonequilibrium diffusion, Phys. Lett. A 272 (2000) 207–217.

[12] S.L. Sobolev, Effects of local nonequilibrium solute diffusion on rapid solidification of alloys, Phys. Status Solidi A 156 (1996) 293–299.

[13] P. Galenko, Extended thermodynamical analysis of a motion of the solid–liquid interface in a rapidly solidifying alloy, Phys. Rev. B 65 (2002) 144103-1-11.

[14] D. Jou, J. Casas-Vazquez, G. Lebon, Extended Irreversible Thermodynamics, second ed., Springer, Berlin, 1996.

[15] R. Trivedi, W. Kurz, Morphological stability of a planar interface under rapid solidification conditions, Acta Metall. 34 (1986) 1663–1670.

[16] P. Galenko, S. Sobolev, Local nonequilibrium effect on undercooling in rapid solidification of alloys, Phys. Rev. E 55 (1997) 343–352.

[17] J. Lipton, W. Kurz, R. Trivedi, Rapid dendrite growth in undercooled alloys, Acta Metall. 35 (1987) 957–964.

[18] W.J. Boettinger, S.R. Coriell, R. Trivedi, in: Mehrabian R., Parrish P.A. (Eds.), Rapid Solidification Processing: Principles and Technologies IV, Claitor's, Baton Rouge, Louisiana, 1988.

[19] D.P. Sekulic, P.K. Galenko, M.D. Krivilyov, L. Walker, F. Gao, Dendritic growth in Al–Si alloys during brazing. Part 2: Computational modeling, Int. J. Heat Mass Transfer 48 (2005) 2385–2396.

[20] P.K. Galenko, D.A. Danilov, Selection of the dynamically stable regime of rapid solidification front motion in an isothermal binary alloy, J. Crystal Growth 216 (2000) 512–536.

[21] M.J. Aziz, T. Kaplan, Acta Metall. 36 (1988) 293–299.